

# **Geophysical Research Letters**

#### RESEARCH LETTER

10.1029/2020GL090197

#### **Key Points:**

- Summertime temperature variance over land increases with local mean temperature in contemporary global climate models
- A theoretical model captures these increases using only projected changes in temperature and relative humidity from global climate models
- Uncertainties in climate sensitivity and plant processes control the spread of climate model summertime temperature variance change

#### **Supporting Information:**

• Supporting Information S1

#### Correspondence to:

L. R. Vargas Zeppetello, lvz7@uw.edu

#### Citation:

Vargas Zeppetello, L. R., & Battisti, D. S. (2020). Projected increases in monthly midlatitude summertime temperature variance over land are driven by local thermodynamics. *Geophysical Research Letters*, 47, e2020GL090197. https://doi.org/10.1029/2020GL090197

Received 4 AUG 2020 Accepted 13 SEP 2020 Accepted article online 21 SEP 2020

## Projected Increases in Monthly Midlatitude Summertime Temperature Variance Over Land Are Driven by Local Thermodynamics

L. R. Vargas Zeppetello<sup>1</sup> and D. S. Battisti<sup>1</sup>

<sup>1</sup>Department of Atmospheric Sciences, University of Washington, Seattle, WA, USA

**Abstract** The increasing frequency of very high temperatures driven by global warming has motivated growing interest in how the probability distribution of summertime temperatures will evolve in the future. Climate models forced by increasing CO<sub>2</sub> simulate increasing monthly-averaged temperature variance across the midlatitudes. In this study we present evidence that these projections are credible and driven primarily by the magnitude of local warming. A first-principles analytic theory reproduces the increased midlatitude summertime temperature variance in climate models extremely well by considering only the warming-induced change in the climatological vapor pressure deficit. The impacts of local warming on saturation specific and relative humidity are shown to have roughly equal contributions to increases in summertime temperature variance. The vegetation response to increasing CO<sub>2</sub> is found to be an important contributor to the uncertainty in modeled temperature variance change, highlighting the role of plants in shaping the summertime temperature distribution.

**Plain Language Summary** Extreme summertime temperatures are a focal point for the impacts of climate change. Climate models driven by increasing  $CO_2$  emissions project increasing summertime temperature variability by the end of the  $21^{st}$  century. If credible, these increases imply that extreme summertime temperatures will become even more frequent than a simple shift in the contemporary probability distribution would suggest. Given the impacts of extreme temperatures on public health, food security, and the global economy, it is of great interest to understand whether the projections of increased temperature variance are credible. In this study, we use a theoretical model of the land surface to demonstrate that the large increases in summertime temperature variance projected by climate models are credible, predictable from first principles, and driven by the effects of warmer temperatures on evapotranspiration. We also find that the response of plants to increased  $CO_2$  and mean warming is important to the projections of increased temperature variability.

### 1. Introduction

How will summertime land surface temperature variability evolve as the climate changes? This question is of paramount importance because it concerns the fundamental coupling between the land surface and the atmosphere and because it has implications for how the frequency of heat waves and droughts will be impacted by a changing background climate. Complicating our understanding of temperature variability over land is the fact that contemporary climate models have significant biases in their representations of historical summertime temperature variance. Figure 1 shows the ratio of the multimodel-mean (MMM) summertime temperature variance of 40 global climate models participating in the Coupled Model Intercomparrison Project Phase 6 (CMIP6 Eyring et al., 2016) to the summertime temperature variance observed over the last 20 years of the historical period (1995-2014). The supporting information contains a list of all models in the ensemble (Table S1). Values greater than 1 in Figure 1 indicate that the historical summertime temperature variance in models is too high. Over a considerable fraction of the midlatitudes, the CMIP6 models analyzed here overpredict temperature variance by at least 20%. This problem has persisted through generations of climate models; similar errors were found in the CMIP5 ensemble (Vargas Zeppetello et al., 2020b). Unfortunately, recent work has shown that the historical biases are not good predictors of how midlatitude summertime temperature variance will evolve in the future, complicating emergent constraint approaches that leverage information about model biases to correct potentially

©2020. American Geophysical Union. All Rights Reserved.

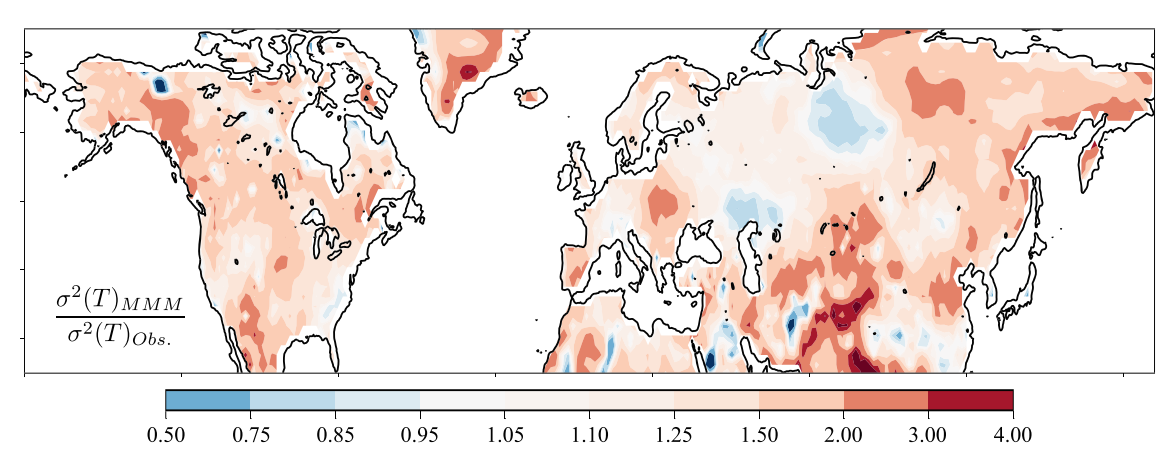


**Figure 1.** Summertime temperature variance bias in climate models defined as the ratio of the multimodel-mean temperature variance from 40 CMIP6 models from 1995–2014 of historical simulations to observed temperature variance from gridded weather station observations from the same period (Willmott & Matsuura, 2001).

faulty projections (Chan et al., 2020). Hence, an assessment of how summertime temperature variance will respond to a warming world is predicated on a mechanistic understanding of the relevant physical processes.

It is widely understood that temperature variability is tied to fluctuations in cloudiness (solar radiation), precipitation, and the turbulent fluxes of heat and moisture at the surface, which are also related to the moisture content of the soil (Berg et al., 2014; Koster et al., 2006; Vogel et al., 2017). The biases in contemporary models and the consensus that soil moisture and surface fluxes are of paramount importance to temperature variability over land (Seneviratne et al., 2010) motivate using simple models of the land surface energy and water budgets to understand the evolution of summertime temperature variance in a warming world.

In recent work, Vargas Zeppetello et al. (2020a) used the local surface energy and water budgets to derive an equation for monthly-averaged summertime temperature variance  $\sigma^2(T')$  as a function of monthly anomalies in shortwave radiation  $\mathcal{F}'$  and precipitation  $\mathcal{P}'$ , as well as two parameters  $\Gamma$  and  $\zeta$  that will be described below:

$$\sigma^{2}(T') = \frac{1}{\Gamma^{2}} \left[ \sigma^{2}(\mathcal{F}') - 2L\zeta \overline{\mathcal{F}'\mathcal{P}'} + (\zeta L)^{2} \sigma^{2}(\mathcal{P}') \right]. \tag{1}$$

In Equation 1, primed quantities represent deviations from monthly mean values in June, July, and August while  $\sigma^2$  terms represent the variance, or average of the squares of these primed anomaly terms. The overbar indicates summertime climatological averages, and L is the latent enthalpy of vaporization (J kg  $H_2O^{-1}$ ). The shortwave variance, precipitation variance, and covariance between monthly anomalies in these two quantities will be referred to as "forcing components," and the spatial pattern of each is shown in the supporting information (Figure S1). Importantly,  $\mathcal{F}'$  and  $\mathcal{P}'$  are not independent; they are anticorrelated (e.g., cloudy months tend to be wetter months), and so the second term on the right-hand side of Equation 1 acts to increase the overall temperature variance. The summertime temperature variance diagnosed by Equation 1 agrees well with the MMM across the CMIP6 historical simulations, the ERA5 reanalysis, and observations across the Northern Hemisphere midlatitudes (Figure S2).

The parameters  $\Gamma$  and  $\zeta$  are functions of the climatological state variables (surface temperature, soil moisture, and atmospheric humidity) and land surface properties (e.g., evaporative resistance and runoff efficiency); equations for both parameters are found in Appendix A1 as part of the derivation of Equation 1.  $\Gamma$  (W m<sup>-2</sup> K<sup>-1</sup>) is an increasing linear function of soil moisture (see Equation A11); this reflects the fact that a greater fraction of incident energy is used for evapotranspiration in wet regions than in dry regions, thereby damping any surface temperature fluctuation associated with a nominal radiation anomaly in wet regions relative to dry regions (Seneviratne et al., 2010, and references therein).  $\zeta$  is the ratio of potential evapotranspiration to the sum of potential evapotranspiration and maximum lateral moisture flux (see Equation A12). This means that  $\zeta$  varies between 0 and 1; in dry regions ( $\zeta \to 1$ ) potential evapotranspiration is high, and precipitation fluctuations are easily converted to temperature anomalies via



evapotranspiration whereas in wet regions ( $\zeta \to 0$ ), high runoff and infiltration rates damp soil moisture fluctuations and mute significant evapotranspiration responses to precipitation fluctuations. This aligns with the literature on soil moisture-temperature interactions: In both observations and models, precipitation-induced soil moisture anomalies preferentially amplify temperature variability in dry regions both because evapotranspiration is more sensitive to soil moisture in regions with low soil moisture and because atmospheric demand for water vapor is higher in dry regions (Koster et al., 2015; Seneviratne et al., 2010).

## 2. Temperature Variance Sensitivity

In this section, we perform a sensitivity analysis of Equation 1 to provide insight into how temperature variance will evolve as the climate warms. Ignoring potential impacts of warming temperatures on the forcing components (which we will analyze later), mean state soil moisture, and model parameters like surface resistance, the partial derivative of Equation 1 with respect to mean summertime temperature  $\overline{T}$  is

$$\frac{\partial \sigma^2(T')}{\partial \overline{T}} = \frac{2}{\Gamma^2} \left[ \left( \zeta \frac{\partial \zeta}{\partial \overline{T}} - \frac{\zeta^2}{\Gamma} \frac{\partial \Gamma}{\partial \overline{T}} \right) L^2 \sigma^2(\mathcal{P}') - \left( \frac{\partial \zeta}{\partial \overline{T}} - \frac{2\zeta}{\Gamma} \frac{\partial \Gamma}{\partial \overline{T}} \right) L \overline{\mathcal{F}'} \overline{\mathcal{P}}' - \frac{1}{\Gamma} \frac{\partial \Gamma}{\partial \overline{T}} \sigma^2(\mathcal{F}') \right]. \tag{2}$$

The three terms on the right-hand side of Equation 2 can be qualitatively understood as the changes to overall temperature variance driven by amplification or damping of the historical patterns of precipitation variance (first term), solar radiation-precipitation covariance (second term), and solar radiation variance (third term). The dependence of  $\zeta$  and  $\Gamma$  on the mean temperature stems from the temperature dependence of the climatological vapor pressure deficit  $\overline{V}$  (also known as the atmospheric water vapor demand). While some of the model parameters and state variables (i.e., stomatal resistance or soil moisture) undoubtedly have complex temperature dependencies, here we only consider the impact of changing climatological demand for water by the atmosphere  $\overline{V}$  due to changes in surface temperature (saturation specific humidity  $q_s(T)$ ) and atmospheric specific humidity:

$$\overline{V} = q_s(\overline{T})(1 - \overline{RH}), \tag{3}$$

where  $\overline{\rm RH}$  is the relative humidity of the overlaying air (see Appendix A1). The sensitivity of the climatological vapor pressure deficit  $\overline{V}$  to mean temperature is

$$\frac{\partial \overline{V}}{\partial \overline{T}} = \frac{dq_s}{d\overline{T}} (1 - \overline{RH}) - q_s(\overline{T}) \frac{\partial \overline{RH}}{\partial \overline{T}}, \tag{4}$$

where the quantity  $\frac{dq_s}{dT}$  is given by the Clausius-Clapeyron relationship. Thus, Equation 2 represents the sensitivity of temperature variance to the impact of climatological warming on saturation specific humidity  $q_s(\overline{T})$  and atmospheric specific humidity (and therefore on relative humidity  $\overline{RH}$ ); saturation specific humidity and relative humidity are the only changing quantities captured by Equation 2.

Maps of the partial derivative  $\frac{\partial \sigma^2(T')}{\partial \overline{T}}$  and the three terms on the right-hand side of Equation 2 are shown in the supporting information (Figures S3a–S3d). The MMM value of the full temperature variance sensitivity (Figure S3d, left-hand side of Equation 2) in both the continental United States and Central Europe ranges from  $0.2^{\circ}\text{C}^{-1}$  to  $0.3^{\circ}\text{C}^{2}$  °C<sup>-1</sup>; this falls within uncertainty estimates of summertime temperature variance change from an empirical analysis of  $\sigma^2(T')$  and  $\overline{T}$  in the CMIP5 ensemble (Chan et al., 2020). The relative importance of each term on the right-hand side of Equation 2 depends on the sign and magnitude of  $\frac{\partial \zeta}{\partial \overline{T}}$  and  $\frac{\partial \Gamma}{\partial \overline{T}}$ . In general, the change in both  $\zeta$  and  $\Gamma$  with respect to mean temperature reflects the tendency toward a more arid climate both through increasing summertime mean saturation specific humidity  $\overline{q}_s$  directly through the Clausius-Clapeyron relationship's temperature dependence and modulating the climatological relative humidity  $\overline{RH}$ . The derivative  $\frac{\partial \zeta}{\partial \overline{T}}$  is generally positive and reflects the fact that a warming mean climate increases potential evapotranspiration everywhere, implying larger precipitation-induced anomalies in evapotranspiration, and hence temperature. The derivative  $\frac{\partial \Gamma}{\partial \overline{T}}$  is more complicated and varies in sign across space; fortunately, this term is small and contributes little to overall temperature variance sensitivity, as can be seen from Figure S3c. The changes in temperature variance that our sensitivity analysis attributes to mean warming manifest almost entirely from the fact that increasing atmospheric water vapor demand driven by mean warming enhances the magnitude of precipitation-induced temperature anomalies.



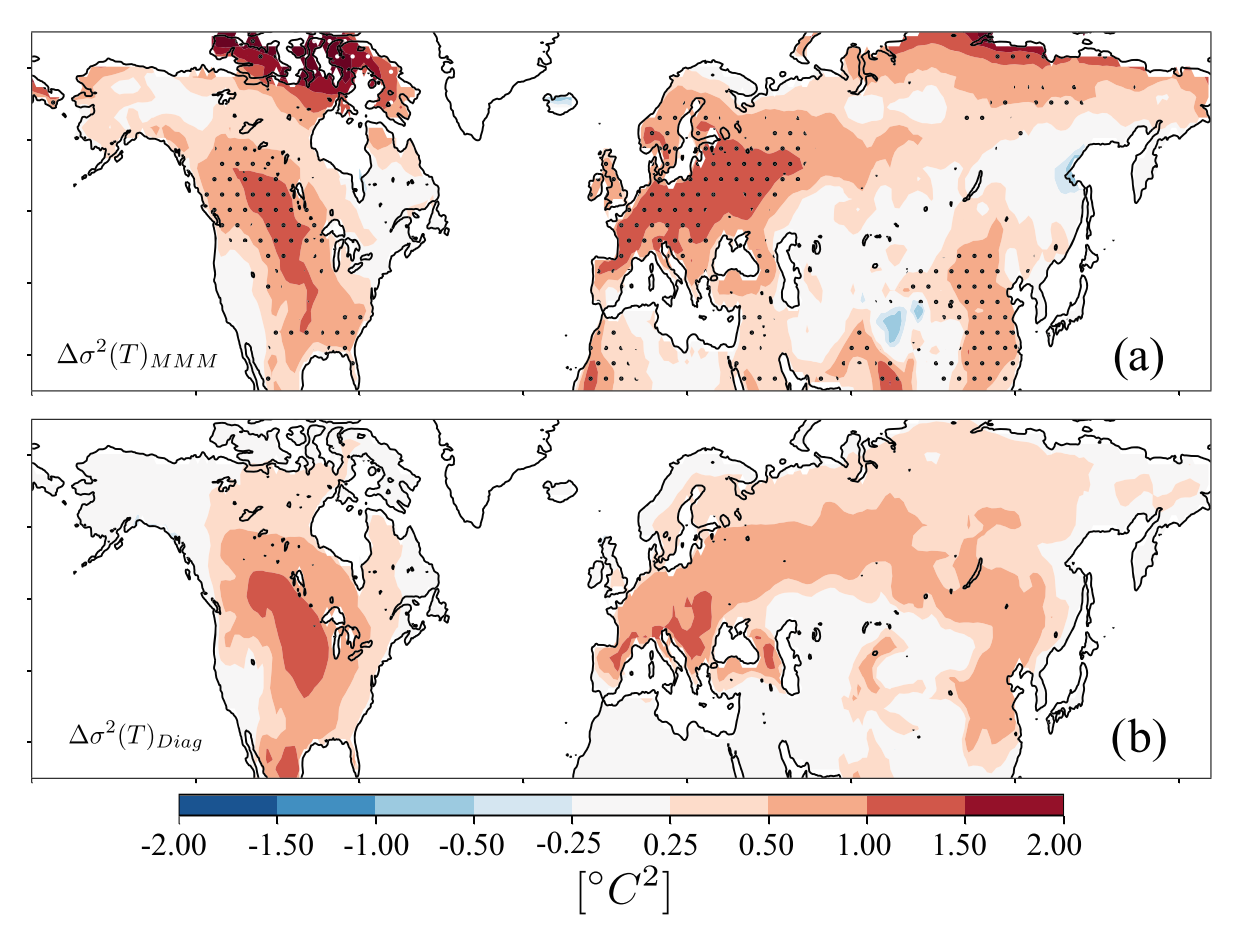


**Figure 2.** The changes in variance of summertime monthly mean temperatures over the 21st century (2080–2099 of the SSP585 emissions scenario minus 1995–2014 of the historical simulations) in the CMIP6 multimodel mean (a) and (b) predicted from Equation 5, which quantifies the impact of the change in mean temperature and atmospheric humidity on temperature variance. Stippling in panel (a) shows regions where more than 75% of the models in the ensemble agree on the sign of the variance change.

### 3. Impact of Mean Warming on Temperature Variance

To calculate the change in temperature variance expected purely from local warming, we compute the sensitivty in Equation 2 using CMIP6 MMM climatological  $\overline{V}$ ,  $\overline{m}$ ,  $\overline{q_s}$ , and  $\overline{\text{RH}}$  from the end of the historical period (1995–2014) shown in Figure S3d. We approximate  $\frac{\partial \overline{\text{RH}}}{\partial \overline{T}}$  by dividing the local MMM relative humidity change at the end of the 21st century by the local MMM warming  $\Delta \overline{T}$ . After calculating the derivatives  $\frac{\partial \zeta}{\partial \overline{T}}$  and  $\frac{\partial \Gamma}{\partial \overline{T}}$  according to Equations A13 and A14, we substitute them into Equation 2 and compute the total change in temperature variance as

$$\Delta \sigma^2(T') = \frac{\partial \sigma^2(T')}{\partial \overline{T}} \Delta \overline{T}.$$
 (5)

Figure 2a shows the CMIP6 MMM change in temperature variance between 2080 and 2099 of the SSP585 simulations (a worst-case anthropogenic emissions scenario that is roughly similar to the RCP8.5 scenario used in AR5) and 1995–2014 of the historical simulations in 24 climate models (see Table S1), while Figure 2b shows the pattern of temperature variance change predicted by Equation 5. The three contributions to temperature variance change from the right-hand side of Equation 2 are shown in the supporting information (Figure S4). The first two terms contribute most of the change; we have discussed above how increasing atmospheric water vapor demand with warming amplifies precipitation-induced temperature anomalies.

The agreement between the variance change projected by our model, which incorporates only the fundamental impact of mean warming on mean atmospheric water vapor demand, and the CMIP6 models is encouraging. Both project a 30–50% increase in temperature variance from the historical period by the end



of the 21st century (a map of the variance increases represented as a percentage is shown in Figure S5). The Central United States, Europe, and East Asia all stand out as regions where the projected impacts of increasing surface temperature variance will be particularly impactful for international food security (Tigchelaar et al., 2018). Further, public health crises driven by extreme heat waves have devastated Europe multiple times since the start of the 20th century (Grumm, 2011; Schär et al., 2004); our results suggest that these heat waves will grow more severe in a warming world as the mean and variance of summertime temperatures increase. The agreement between our model and the CMIP6 ensemble suggests that despite the large biases present in the temperature variance of CMIP6 historical simulations, the *changes* projected by the climate models are credible and should be accounted for in policy that seeks to make populations and food systems throughout the midlatitudes more resilient to extreme temperature shocks.

## 4. Changes in Surface Insolation and Precipitation Variability

Our analysis captures a fundamental impact of climate change on land surface climate because the impact of warming on  $q_s(\overline{T})$  is governed by the Clausius-Clapeyron relationship and is therefore model independent. We hypothesize that the model invariant nature of the warming impact we isolate in Equation 2 is the reason why the MMM pattern of temperature variance change agrees well with our estimate shown in Figure 2b. However, Equation 2 does not take into account changes in the forcing components  $(\Delta\sigma^2(\mathcal{F}'), \Delta\mathcal{F}'\mathcal{P}', \Delta\sigma^2(\mathcal{P}'))$ , changes in mean soil moisture  $(\Delta\overline{m})$ , or changes in other model parameters like stomatal resistance that may play significant roles in the changes to temperature variance that manifest within particular models. We left these changes out of our sensitivity analysis because each of these changes can be viewed as responses to warming rather than a truly independent forcing; for example, a reduction in mean relative humidity is likely to be accompanied by a reduction in mean cloudiness, an increase in mean insolation, and therefore a reduction in mean surface soil moisture and shortwave radiation variance (Laguë et al., 2019).

To estimate the impact of the changes in shortwave and precipitation variability in the CMIP6 models (see Figure S6) on the changes in temperature variance, we use Equation 1, plugging in the forcing at the end of the 21st century and the end of the 20th century—in both cases keeping all state variables and parameter values equal to their historical (end of the 20th century) values. The difference between these two calculations isolates the impact of changes to the forcing components on temperature variance and is shown in Figure S7. The impact of changes to the forcing components is of similar magnitude to the MMM change due solely to mean warming shown in Figure 2b, but with a different spatial pattern than that shown in Figures 2a and 2b. That the impact of changes to the forcing components is unrelated to the MMM temperature variance change suggests some compensatory mechanisms that operate within each model to counteract the large temperature variance changes that would result from the changing in forcing alone (e.g., changes in climatological soil moisture and stomatal resistance).

Evidence that compensatory mechanisms effectively cancel out the large changes in temperature variance expected from the changes in forcing across models can be seen by examining the spread in the change in temperature variance projections within the CMIP6 ensemble (shown in Figure S8a). The spread across models in projected temperature variance changes due to changes in the forcing components (Figure S8c, obtained by using each model's forcing changes individually in the same manner that Figure S7 was generated) is much greater than the spread in the change in temperature variance simulated by the CMIP6 models themselves—the later being consistent in amplitude and pattern with that calculated using only the spread in the change in the mean temperature and humidity with Equation 2 (Figure S8b). The much larger uncertainty in the temperature variance change due to the spread in the forcing-induced variance change alone, combined with the lack of agreement between the MMM temperature variance change pattern (Figure 2a) and the estimate of temperature variance change driven purely by the MMM changes in forcing (Figure S7), strongly suggests that the competing effects of changing forcing, soil moisture, and underlying model parameters—while individually large—largely oppose one another. Therefore, the change in temperature variance that manifests uniformly and robustly across the models is due to the model invariant impact of mean warming on atmospheric-specific humidity and surface saturation-specific humidity that is captured by our sensitivity analysis.



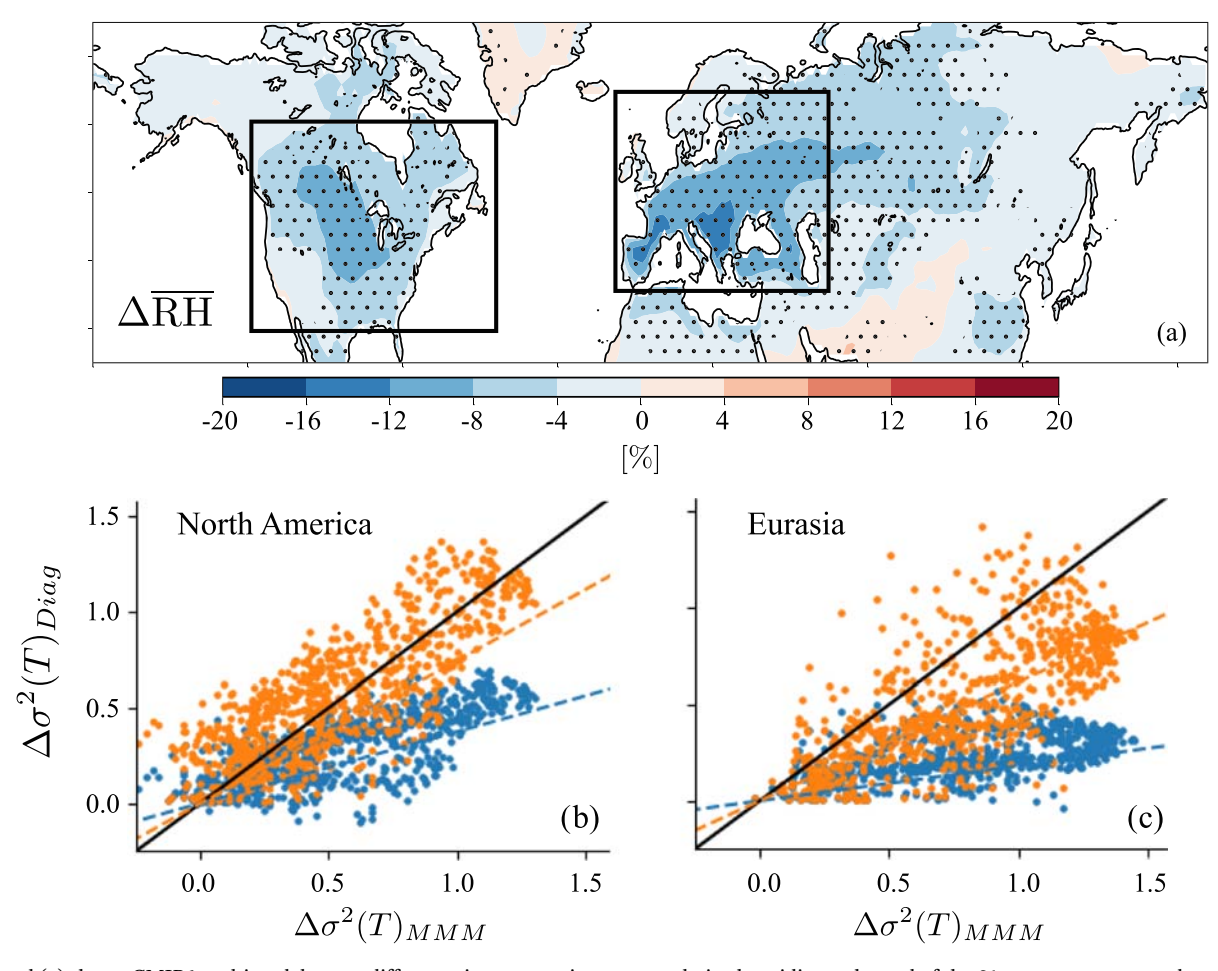


**Figure 3.** Panel (a) shows CMIP6 multimodel-mean difference in summertime mean relative humidity at the end of the 21st century compared to the end of the 20th century. Stippling shows grid cells where 75% of models agree on the sign of the change. Panels (b) and (c) show comparisons between our prediction of temperature variance change based on Equation 5 (*y* axis) and the multimodel-mean values (*x* axis) in North America and Eurasia, respectively (regions are defined by the black boxes in panel a). Orange dots show the calculation if the change in relative humidity is accounted for; blue dots show the calculation when the value of  $\frac{\partial \overline{RH}}{\partial T}$  is artificially set to zero. The black solid line has slope 1, and the dashed lines are a least squares fit.

#### 5. The Importance of Relative Humidity in Temperature Variance Projections

Using only changes in local summertime mean temperature and relative humidity, our sensitivity analysis reproduces the projected changes in summertime temperature variance in the CMIP6 models. The MMM change in relative humidity is shown in Figure 3a; stippling shows grid cells where more than 75% of the models agree on the sign of the change. To understand the relative contribution of local relative humidity changes to the increased temperature variance, we can artificially set  $\frac{\partial \mathrm{RH}}{\partial T} = 0$  in Equation 4 and recalculate  $\Delta \sigma^2(T')$  in North America and Eurasia, two regions where the changes in relative humidity are large and robust across models.

The dots in Figures 3b and 3c show the temperature variance changes predicted by the full version of Equation 2 (orange) and the artificial prediction where relative humidity changes are excluded from the analysis (blue) as a function of the MMM value of  $\Delta\sigma^2(T')$ . In both regions, relative humidity changes are equally important as local warming to the projected increase in temperature variance. Both local warming and decreasing relative humidity act to amplify the local atmospheric water vapor demand. In regions where soil moisture is plentiful due to large annually averaged rainfall (like Eurasia and the central United States), increased atmospheric demand for water vapor allows for large evapotranspiration anomalies that amplify precipitation-induced temperature anomalies and therefore increase temperature variance.

Relative humidity changes are of first-order importance to the increased summertime temperature variance projected by climate models in the CMIP6 ensemble, but to what extent does local warming control changes



in relative humidity over land? Byrne and O'Gorman (2018) have argued that the change in relative humidity over land surfaces is primarily a product of the differential warming over land and ocean. If this were true, the dominant control of model climate sensitivity on the regional warming patterns found across contemporary climate models suggests that model differences in surface warming should account for differences in the change in local relative humidity over land. Figure S9 shows the changes in local relative humidity as a function of local mean temperature changes averaged across the two boxed regions in Figure 3a. Nearly half of the variance in relative humidity changes across models (46%) is explained by the local warming over North America, while in Eurasia 31% of the variance is explained by local warming. While local warming is clearly a strong predictor of local changes in relative humidity, other mechanisms are required to explain the intermodel spread within the CMIP6 ensemble.

## 6. Plant Activity and Summertime Temperatures

Arora et al. (2019) have calculated sensitivity parameters that quantify the global response of the carbon cycle to increasing  $CO_2$  and temperatures in 10 of the models analyzed in this study (see Table S1). Such parameters combine numerous plant physiological responses to increasing temperature and atmospheric  $CO_2$  such as increased leaf area, stomatal closure, and a changing growing season start date. The carbon-concentration feedback parameter  $\beta$  quantifies global ecosystem response to only a change in atmospheric  $CO_2$  (without the associated warming): A greater  $\beta$  implies a greater increase in carbon uptake by the land surface in response to increasing  $CO_2$  emissions. One pathway for a greater  $\beta$  that is of interest to our study is an increase in leaf area driven by a higher atmospheric  $CO_2$  concentration, which would increase the mean evapotranspiration. The carbon-climate feedback parameter  $\gamma$  quantifies the global ecosystem response to a changing mean temperature (without the associated impacts of increased  $CO_2$  concentrations). The table inset in Figure S9 shows that the carbon-concentration feedback value  $\beta$  is well correlated with relative humidity change in both Eurasia and North America and that  $\beta$  explains a similar amount of variance in  $\Delta \overline{RH}$  across models as mean warming  $\Delta \overline{T}$ .

Across models, the vegetation response to increasing atmospheric  $CO_2$  is important for the projections of future carbon sequestration and for changes in local mean relative humidity and, by extension, summertime temperature variance. In models with a large positive carbon-concentration feedback parameter  $\beta$ , the vegetation response to increased  $CO_2$  concentrations mutes the response of  $\overline{RH}$ —likely by increasing evapotranspiration through an increase in leaf area. Models with a larger leaf area response will therefore exhibit smaller increases in temperature variance due to the mitigating effects of changes in vegetation on the climatological relative humidity change. Differences in the plant response to warming (quantified by the  $\gamma$  parameter values from Arora et al., 2019) explain more than 10% of the model spread in the climatological relative humidity change in North America; this suggests that in models where plants are more sensitive to warming, they can mitigate the increase in temperature variance associated with warming by reducing the climatological drying of the atmosphere, perhaps by way of earlier leaf-out dates in spring-time (Xu et al., 2020). In general, the spread in the climatological local warming combined with the plant response to climate change explains nearly all of the intermodel differences in the projected change in land summertime mean relative humidity.

## 7. Conclusions

A theoretical model of monthly-averaged temperature variability based on the land surface energy and water budgets shows that the projected changes in the CMIP6 MMM summertime temperature variance in the SSP585 scenario are driven by the impact of local mean warming on atmospheric water vapor demand at the land surface. Despite the high biases in summertime temperature variance present in the CMIP6 models' representation of the historical period (Figure 1), the model projections of increased monthly-averaged summertime temperature variance are credible and reproducible from a theoretical model of the land surface energy and moisture budgets. While uncertainty in changes to the radiative forcing, precipitation, soil moisture, and other land surface parameters are undoubtedly influential on temperature variance within each particular model, the pattern that manifests in the MMM is driven by the model invariant response of atmospheric vapor pressure deficit that is governed by the Clausius-Clapeyron relationship.

We have identified several uncertainties in how summertime temperature variance will change: the magnitude of local mean warming, which is primarily controlled by model climate sensitivity; the plant



physiological response to  $\mathrm{CO}_2$  emissions and how that response changes with mean climate warming; and changes in the atmospheric forcings that are governed by cloud and precipitation parameterizations that differ across models. In particular, we have shown that models with strong positive land-carbon cycle responses to increasing atmospheric  $\mathrm{CO}_2$  simulate smaller reductions in mean relative humidity than do models with weak land-carbon responses, indicating that plant activity mitigates the projected reductions in relative humidity that are driven by increasing temperature.

Local warming and the plant response to climate change are the primary contributors to how monthly-averaged summertime temperature variability will increase in the future. The simple model and the CMIP6 MMM predict that changes in summertime temperature variance will be greater than  $1^{\circ}$ C<sup>2</sup> across much of Eurasia and central North America, representing a 30–50% increase in historical temperature variance in these regions. Though an assessment of the impacts these kinds of increases in variability would have on the frequency of food shocks and deadly heatwaves is outside the scope of this study, the compounding impacts of a mean warming and increasingly temperature variability warrant future study and likely serious policy attention.

## **Appendix A: Methods**

This section presents a derivation of Equation 1, but interested readers can find a more detailed presentation in Vargas Zeppetello et al. (2020a). Briefly, this model uses only three tunable parameters to generate an estimate of summertime temperature variance based on monthly anomalies of net solar radiation  $\mathcal{F}'$  and precipitation  $\mathcal{P}'$ . Each of these parameters will be defined in the course of this brief derivation.

We begin with the assumption that on monthly timescales the land surface energy and water budgets are approximately in equilibrium:

$$0 \approx \mathcal{F}' - F'_{IW} - LE' - H' - G', \tag{A1}$$

$$0 \approx \mathcal{P}' - E' - R' - I'. \tag{A2}$$

All terms in Equation A1 are given in W m<sup>-2</sup>, while all terms in Equation A2 are given in kg  $H_2O$  m<sup>-2</sup> s<sup>-1</sup>.  $F_{LW}$  is the net upward surface longwave radiation flux, H is the upward turbulent flux of sensible heat, and G is the flux of energy downward into the soil column. R and I are the surface runoff and infiltration moisture fluxes, respectively; E is the net evapotranspiration; and E is the latent enthalpy of vaporization.

We assume that the sum of monthly net longwave, sensible heat, and ground heat flux anomalies is linearly proportional to temperature fluctuations, thus

$$F'_{IW} + H' + G' = \nu T'. \tag{A3}$$

The first model parameter,  $\nu$  (W m<sup>-2</sup> K<sup>-1</sup>) controls the response of 2-m air temperature T' to a radiative forcing  $\mathcal{F}'$  in the absence of evapotranspiration anomalies (see Equation A1). We assume  $\nu$  to be constant over the land surface and insensitive to any change in climate.

The sum of runoff and infiltration anomalies is assumed to be linearly proportional to soil moisture fluctuations, thus

$$R' + I' = \mu m'. \tag{A4}$$

The fractional surface saturation m is a unitless number between zero and one that designates the fraction of available pore space in the evapotranspiration-accessible portion of the soil column that is occupied by liquid water. To ensure proper scaling between runoff, infiltration, and precipitation, we set the "surface moisture capacity"  $\mu$  (kg m<sup>-2</sup> s<sup>-1</sup>) to be

$$\mu = \eta \overline{\mathcal{P}},\tag{A5}$$

where  $\overline{P}$  is the summertime mean monthly-averaged precipitation at each grid cell over the historical period (1995–2014) and  $\eta$  is a unitless parameter that controls the mass of liquid water required to effectively change the soil's fractional saturation m that we assume to be spatially uniform.



Total evapotranspiration is given by

$$E = \frac{\rho_a}{r_s} mV. \tag{A6}$$

In Equation A6,  $\rho_a$  (kg air m<sup>-3</sup>) is the density of air;  $r_s$  (s m<sup>-1</sup>) is the "bulk surface resistance" parameter; V (kg H<sub>2</sub>O kg air<sup>-1</sup>) is a measure of the atmospheric demand for water vapor  $q_s(T) - q$ , where  $q_s$  is the saturation-specific humidity at the 2-m air temperature T; and q is the boundary layer specific humidity. As Equations A1 and A2 are written in terms of anomalies, we take the first-order terms in a Taylor expansion of Equation A6 as follows:

$$E' = \frac{\rho_a}{r_s} \left[ m' \overline{V} + \overline{m} \frac{dq_s}{dT} T' \right], \tag{A7}$$

where barred terms indicate summertime mean values. In Equation A7, we have made use of observations and model results that show that anomalies in  $\overline{V}$  are overwhelmingly due to anomalies in  $q_s$  (rather than q) (van Heerwaarden et al., 2010). By substituting Equation A7 into Equation A2, we obtain

$$m' = \frac{1}{\mu + \delta} \left[ \mathcal{P}' - \frac{\rho_a \overline{m}}{r_s} \frac{dq_s}{dT} T' \right],\tag{A8}$$

where we have defined

$$\delta = \frac{\rho_a \overline{V}}{r_s} \tag{A9}$$

as the climatological mean potential evapotranspiration, or the mean evapotranspiration  $\overline{E}$  expected for  $\overline{m}=1$ , or saturated soils (see Equation A6). The climatological mean vapor pressure deficit can be written  $\overline{V}=q_s(\overline{T})(1-\overline{RH})$ , where  $\overline{RH}$  is the climatological relative humidity. Note that  $\delta$  increases exponentially with  $\overline{T}$  according to the Clausius-Clapeyron relationship.

Combining Equation A8 with Equations A1, A3, and A7, we obtain

$$T' = \frac{1}{\Gamma} [\mathcal{F}' - \zeta L \mathcal{P}']. \tag{A10}$$

The square of Equation A10 gives Equation 1, which is the starting point of our analysis in this paper. The  $\Gamma^{-1}$  parameter defines the land surface's "moist surface climate sensitivity" and scales with mean soil moisture:

$$\Gamma = \nu + \frac{L\rho_a \overline{m}}{r_s} \frac{dq_s}{dT} (1 - \zeta), \tag{A11}$$

while  $\zeta$  is given as

$$\zeta = \frac{\delta}{\delta + \mu}.\tag{A12}$$

The  $\zeta$  parameter is the ratio of potential evapotranspiration  $\delta$  to the sum of potential evapotranspiration and lateral moisture flux  $\mu$ . The  $\zeta$  parameter is thus a measure of climatological surface dryness and varies between 0 and 1 at each point in space. Places with  $\zeta\approx 1$  have extremely large potential evapotranspiration  $\delta$  compared to the intermittent supply of water by precipitation, indicating an extremely hot and dry land surface. In contrast, places with smaller  $\zeta$  have low potential evapotranspiration; these occur primarily in extremely in humid regions with large amounts of rainfall. Both of these parameters include saturation-specific humidity  $q_s(T)$ , the dependence on temperature of which is articulated through the Clausius-Clapeyron relationship. From Equations A11 and A12, we can compute their partial derivatives with respect to temperature as follows:

$$\frac{\partial \zeta}{\partial \overline{T}} = \frac{\mu}{(\delta + \mu)^2} \left( \frac{d\overline{q_s}}{d\overline{T}} (1 - \overline{RH}) - \overline{q_s} \frac{\partial \overline{RH}}{\partial \overline{T}} \right), \tag{A13}$$

$$\frac{\partial \Gamma}{\partial \overline{T}} = \frac{L\rho_a \overline{m}}{r_s} \left( \frac{d^2 \overline{q_s}}{d \overline{T}^2} (1 - \zeta) - \frac{d \overline{q_s}}{d \overline{T}} \frac{\partial \zeta}{\partial \overline{T}} \right). \tag{A14}$$



The differentials in Equations A13 and A14 reflect different impacts of mean temperature change on local thermodynamics that impact the energetics of evapotranspiration.

## **Data Availability Statement**

Data sets for this research are available in this in-text data citation reference: (Eyring et al., 2016), with license of CMIP6. Analysis codes and processed data for generating figures in this study are posted at Zenodo (https://zenodo.org/record/3877318#.XtqiG55KhTY).

#### Acknowledgments

This paper contains data from the NOAA ESRL and the CMIP6 data archive. We are grateful to all who made these data available to the public. The EcoClimate group at the University of Washington provided invaluable feedback during the development of the diagnostic equation and preparation of the manuscript. Marcia Baker helped develop the model and provided feedback on the text of this manuscript. We are also grateful to three reviewers whose comments greatly improved the manuscript. L. R. V. Z. was supported by a NSF GRFP Fellowship, and D. S. B. was supported by a grant from the Tamaki Foundation.

#### References

- Arora, V. K., Katavouta, A., Williams, R. G., Jones, C. D., Brovkin, V., Friedlingstein, P., et al. (2019). Carbon-concentration and carbon-climate feedbacks in CMIP6 models, and their comparison to CMIP5 models. *Biogeosciences Discussions*, 2019, 1–124. https://doi.org/10.5194/bg-2019-473
- Berg, A., Lintner, B. R., Findell, K. L., Malyshev, S., Loikith, P. C., & Gentine, P. (2014). Impact of soil moisture-atmosphere interactions on surface temperature distribution. *Journal of Climate*, 27(21), 7976–7993. https://doi.org/10.1175/JCLI-D-13-00591.1
- Byrne, M. P., & O'Gorman, P. A. (2018). Trends in continental temperature and humidity directly linked to ocean warming. *Proceedings of the National Academy of Sciences*, 115(19), 4863–4868. https://doi.org/10.1073/pnas.1722312115
- Chan, D., Cobb, A., Zeppetello, L. R. V., Battisti, D. S., & Huybers, P. (2020). Summertime temperature variability increases with local warming in midlatitude regions. *Geophysical Research Letters*, 47, e2020GL087624. https://doi.org/10.1029/2020GL087624
- Eyring, V., Bony, S., Meehl, G. A., Senior, C. A., Stevens, B., Stouffer, R. J., & Taylor, K. E. (2016). Overview of the Coupled Model Intercomparison Project Phase 6 (CMIP6) experimental design and organization. *Geoscientific Model Development*, 9(5), 1937–1958. https://doi.org/10.5194/gmd-9-1937-2016
- Grumm, R. H. (2011). The Central European and Russian Heat Event of July–August 2010. Bulletin of the American Meteorological Society, 92(10), 1285–1296. https://doi.org/10.1175/2011BAMS3174.1
- Koster, R., Salvucci, G., Rigden, A., Jung, M., Collatz, G., & Schubert, S. (2015). The pattern across the continental United States of evapotranspiration variability associated with water availability. Frontiers in Earth Science, 3, 35. https://doi.org/10.3389/feart.2015. 00035
- Koster, R. D., Suarez, M. J., & Schubert, S. D. (2006). Distinct hydrological signatures in observed historical temperature fields. *Journal of Hydrometeorology*, 7(5), 1061–1075. https://doi.org/10.1175/JHM530.1
- Laguë, M. M., Bonan, G. B., & Swann, A. L. S. (2019). Separating the impact of individual land surface properties on the terrestrial surface energy budget in both the coupled and uncoupled land-atmosphere system. *Journal of Climate*, 32(18), 5725–5744. https://doi.org/10. 1175/JCLI-D-18-0812.1
- Schär, C., Vidale, P. L., Luthi, D., Frei, C., Häberli, C., Liniger, M. A., & Appenzeller, C. (2004). The role of increasing temperature variability in European summer heatwaves. *Nature*, 427(6972), 332–366. https://doi.org/10.1038/nature02300
- Seneviratne, S. I., Corti, T., Davin, E. L., Hirschi, M., Jaeger, E. B., Lehner, I., et al. (2010). Investigating soil moisture-climate interactions in a changing climate: A review. *Earth Science Reviews*, 99(3), 125–161.
- Tigchelaar, M., Battisti, D. S., Naylor, R. L., & Ray, D. K. (2018). Future warming increases probability of globally synchronized maize production shocks. *Proceedings of the National Academy of Sciences*, 115(26), 6644–6649. https://doi.org/10.1073/pnas.1718031115
- van Heerwaarden, C. C., Vilà-Guerau de Arellano, J., Gounou, A., Guichard, F., & Couvreux, F. (2010). Understanding the daily cycle of evapotranspiration: A method to quantify the influence of forcings and feedbacks. *Journal of Hydrometeorology*, 11(6), 1405–1422. https://doi.org/10.1175/2010JHM1272.1
- Vargas Zeppetello, L. R., Battisti, D. S., & Baker, M. B. (2020a). A new look at the summertime temperature variance over land. *Journal of Climate*, 33, 5465–5477. https://doi.org/10.1175/JCLI-D-19-0887.1
- Vargas Zeppetello, L. R., Tétreault-Pinard, E., Battisti, D. S., & Baker, M. B. (2020b). Identifying the sources of continental summertime temperature variance using a diagnostic model of land-atmosphere interactions. *Journal of Climate*, 33(9), 3547–3564. https://doi.org/10.1175/ICLI-D-19-0276.1
- Vogel, M. M., Orth, R., Cheruy, F., Hagemann, S., Lorenz, R., van den Hurk, B. J. J. M., & Seneviratne, S. I. (2017). Regional amplification of projected changes in extreme temperatures strongly controlled by soil moisture-temperature feedbacks. *Geophysical Research Letters*, 44, 1511–1519. https://doi.org/10.1002/2016GL071235
- Willmott, C. J., & Matsuura, K. (2001). Terrestrial air temperature and precipitation: Monthly and annual time series (1900–2017) V5.01. http://climate.geog.udel.edu/climate/htmlpages/README.ghcnts2.html
- Xu, X., Riley, W. J., Koven, C. D., Jia, G., & Zhang, X. (2020). Earlier leaf-out warms air in the north. *Nature Climate Change*, 10, 370–375. https://doi.org/10.1038/s41558-020-0713-4